JVI Journals.ASM.org

A 2.5-Kilobase Deletion Containing a Cluster of Nine MicroRNAs in the Latency-Associated-Transcript Locus of the Pseudorabies Virus Affects the Host Response of Porcine Trigeminal Ganglia during Established Latency

Nada Mahjoub,[a,b] Sophie Dhorne-Pollet,[a,b] Walter Fuchs,[c] Marie-Laure Endale Ahanda,[a,b] Elke Lange,[c] Barbara Klupp,[c] Anoop Arya,[a,b] Jane E. Loveland,[d] François Lefevre,[e] Thomas C. Mettenleiter,[c] Elisabetta Giuffra[a,b]

INRA, AgroParisTech, UMR1313 Animal Genetics and Integrative Biology, Jouy-en-Josas, France[a]; CEA, DSV, IRCM, SREIT, LREG, Jouy-en-Josas, France[b]; Friedrich-Loeffler-Institut, Federal Research Institute for Animal Health, Greifswald-Insel Riems, Germany[c]; Computational Genomics, Wellcome Trust Sanger Institute, Wellcome Trust Genome Campus, Hinxton, United Kingdom[d]; INRA, Molecular Immunology and Virology Unit, Jouy-en-Josas, France[e]

ABSTRACT

The alphaherpesvirus pseudorabies virus (PrV) establishes latency primarily in neurons of trigeminal ganglia when only the transcription of the latency-associated transcript (LAT) locus is detected. Eleven microRNAs (miRNAs) cluster within the LAT, suggesting a role in establishment and/or maintenance of latency. We generated a mutant (M) PrV deleted of nine miRNA genes which displayed properties that were almost identical to those of the parental PrV wild type (WT) during propagation *in vitro*. Fifteen pigs were experimentally infected with either WT or M virus or were mock infected. Similar levels of virus excretion and host antibody response were observed in all infected animals. At 62 days postinfection, trigeminal ganglia were excised and profiled by deep sequencing and quantitative RT-PCR. Latency was established in all infected animals without evidence of viral reactivation, demonstrating that miRNAs are not essential for this process. Lower levels of the large latency transcript (LLT) were found in ganglia infected by M PrV than in those infected by WT PrV. All PrV miRNAs were expressed, with highest expression observed for prv-miR-LLT1, prv-miR-LLT2 (in WT ganglia), and prv-miR-LLT10 (in both WT and M ganglia). No evidence of differentially expressed porcine miRNAs was found. Fifty-four porcine genes were differentially expressed between WT, M, and control ganglia. Both viruses triggered a strong host immune response, but in M ganglia gene upregulation was prevalent. Pathway analyses indicated that several biofunctions, including those related to cell-mediated immune response and the migration of dendritic cells, were impaired in M ganglia. These findings are consistent with a function of the LAT locus in the modulation of host response for maintaining a latent state.

IMPORTANCE

This study provides a thorough reference on the establishment of latency by PrV in its natural host, the pig. Our results corroborate the evidence obtained from the study of several LAT mutants of other alphaherpesviruses encoding miRNAs from their LAT regions. Neither PrV miRNA expression nor high LLT expression levels are essential to achieve latency in trigeminal ganglia. Once latency is established by PrV, the only remarkable differences are found in the pattern of host response. This indicates that, as in herpes simplex virus, LAT functions as an immune evasion locus.

Pseudorabies virus (PrV) is a porcine alphaherpesvirus. The genome of PrV is more than 142 kb in size and is characterized by the presence of 70 different coding genes plus the latency-associated transcript (LAT) locus (1, 2). PrV is the etiological agent of Aujeszky's disease, causing neurological, respiratory, and reproductive disease in the pig, its natural host. Despite successful vaccination campaigns and eradication of the virus from various countries, pseudorabies outbreaks still occur in swine populations worldwide, as recently reported from China (3). Because latent infection persists for lifetime after recovery from acute disease, pigs latently infected by PrV are a constant danger for virus reactivation, shedding, and spread in susceptible populations (4–6).

A particular feature of herpesviruses is their ability to establish and maintain latent infections in which the virus genome circularizes and persists as an episome. As for other alphaherpesviruses, neurons in the trigeminal ganglia are the primary site of PrV latency (7). Over this period, transcription of viral lytic genes is repressed and transcription of the viral genome is restricted to the LAT locus overlapping the internal repeat sequence (IR) (8–10). RNAs of multiple sizes are transcribed from the strand opposite that encoding EP0 and IE180, which can be detected in infected

Received 25 July 2014 **Accepted** 9 October 2014

Accepted manuscript posted online 15 October 2014

Citation Mahjoub N, Dhorne-Pollet S, Fuchs W, Endale Ahanda M-L, Lange E, Klupp B, Arya A, Loveland JE, Lefevre F, Mettenleiter TC, Giuffra E. 2015. A 2.5-kilobase deletion containing a cluster of nine microRNAs in the latency-associated-transcript locus of the pseudorabies virus affects the host response of porcine trigeminal ganglia during established latency. J Virol 89:428–442. doi:10.1128/JVI.02181-14.

Editor: L. M. Hutt-Fletcher

Address correspondence to Elisabetta Giuffra, elisabetta.giuffra@jouy.inra.fr.

N.M. and S.D.-P. contributed equally to this work.

Supplemental material for this article may be found at http://dx.doi.org/10.1128/JVI.02181-14.

doi:10.1128/JVI.02181-14

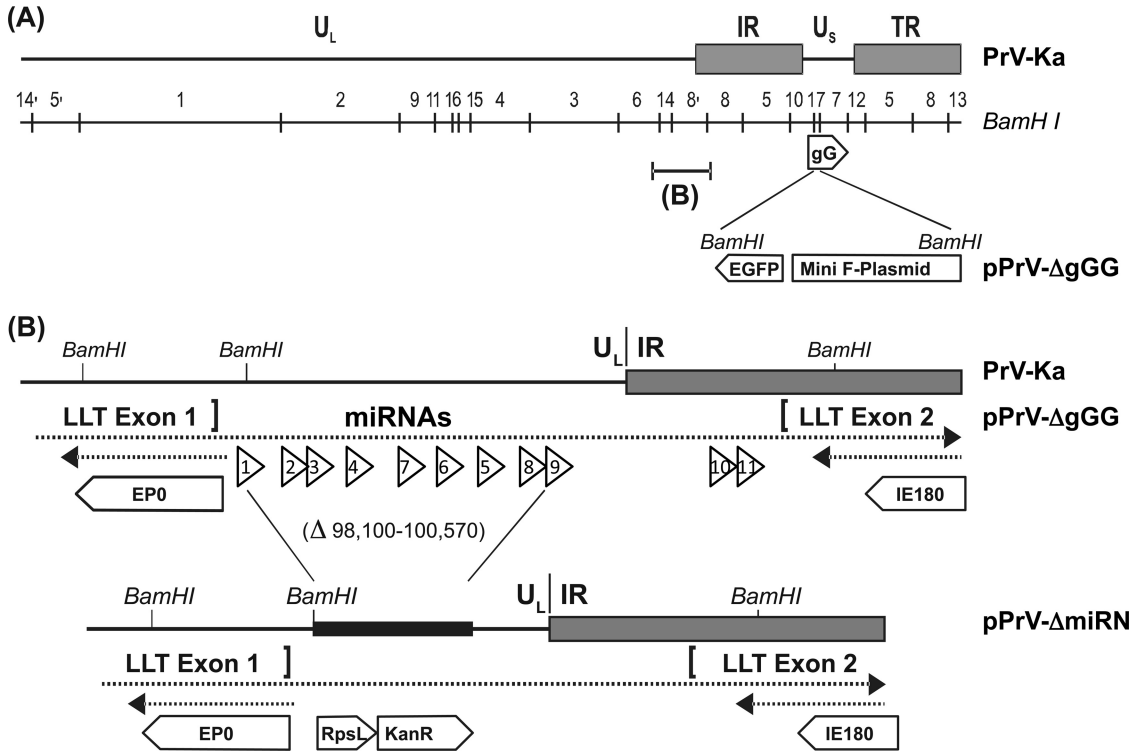

FIG 1 (A) Physical map of the PrV-Ka genome containing unique (U_L and U_S) and inverted repeat (IR and TR) sequences. BamHI restriction sites and fragments, as well as the insertion of a bacterial vector and of an EGFP reporter gene cassette at the gG gene locus in pPrV-ΔgGG (24), are indicated. (B) An enlarged section shows the boundary between U_L and I_R with the open reading frames of the regulatory proteins EP0 and IE180. Viral mRNAs and the spliced large latency transcript (LLT) are indicated by dotted arrows. Identified miRNAs (22, 23) are shown as arrowheads numbered from 1 to 11 (corresponding to miRNA genes from prv-mir-LLT1 to prv-mir-LLT11). In pPrV-ΔmiRN, the majority of the miRNA genes were deleted and replaced by selection markers (RpsL and KanR) used for BAC mutagenesis in *E. coli*.

swine trigeminal ganglia (8, 10, 11). The largest is the 8.4-kb large latency transcript (LLT). Transcription from the LAT region also occurs during lytic infection of cultured mammalian cells, although a different set of transcripts is expressed (12).

MicroRNAs (miRNAs) are small noncoding RNAs of approximately 22 nucleotides (nt) that regulate gene expression posttranscriptionally. By complete or partial hybridization, miRNAs induce target mRNA degradation and/or translational repression; thus, they serve key roles in the regulation of almost every important cellular process in multicellular eukaryotes (13–15). Given their small size, their lack of antigenicity, and their ability to inhibit the translation of specific mRNA species, miRNAs are thought to represent ideal tools for viruses to establish conditions permissive for viral replication, for the establishment of latency, or to allow rapid responses to changes in the environment, such as those that trigger reactivation from latency (16–18). The first viral miRNA was identified in Epstein-Barr virus (EBV), a gammaherpesvirus (19). With advances in sequencing technologies, the identification of miRNAs in many human and animal herpesviruses rapidly followed (17, 20).

Several alphaherpesviruses have been reported to encode miRNAs, which often are clustered in the viral genome, map within the LAT locus or in adjacent regions, and are found encoded on both strands (20, 21). In PrV, a cluster of 11 miRNA genes has been identified by deep sequencing in porcine immature dendritic cells (22) and in a porcine kidney (PK15) cell line (23) during lytic infection. This cluster is entirely contained within the ~4.6-kb intron of the LLT, which functions as a primary miRNA precursor (23).

Here, we report the results of an experimental infection to assess the importance of an miRNA-containing region for the establishment of PrV latency in its natural porcine host. To this end, we generated a PrV mutant deleted of a 2.5-kb portion of the LLT intron harboring nine miRNA genes. We adopted a deep sequencing approach to characterize the transcriptional profiles of trigeminal ganglia focusing on miRNAs and coding genes.

MATERIALS AND METHODS

Construction of virus mutants. The virus generated in this study was derived from the green fluorescent protein (GFP)-expressing mutant pPrV-ΔgGG (24), which contains the genome of PrV strain Kaplan (PrV-Ka) (25) cloned as a bacterial artificial chromosome (BAC).

To delete the miRNA cluster, pPrV-ΔgGG (Fig. 1A) was mutagenized in *Escherichia coli* using the counterselection BAC modification kit (Gene Bridges). The provided selection cassette conferring streptomycin sensitivity (RpsL) and kanamycin resistance (KanR) was amplified by PCR (Pfx DNA polymerase; Life Technologies) with primers PDMIRN-F (5′-CGG TGGGTCGACGGCTCCTGGGGCTGAAAGCGGCGCTGCGGATCC CCCGCggcctggtgatgatggcgggatcg-3′) and PDMIRN-R (5′-GTGTGCGT GTGCGAGAGAGAA GAGATGCGGGGGAGGGCGGCGGGCGCTTGt cagaagaactcgtcaagaaggcg-3′), which contained 5′ extensions (uppercase letters) corresponding to nucleotides 98050 to 98099 and the reversal of nucleotides 100571 to 100620 of the PrV-Ka genome sequence, respectively (GenBank accession number JQ809328) (26). The 1,419-bp PCR product was used for Red/ET-mediated recombination with pPrV-ΔgGG,

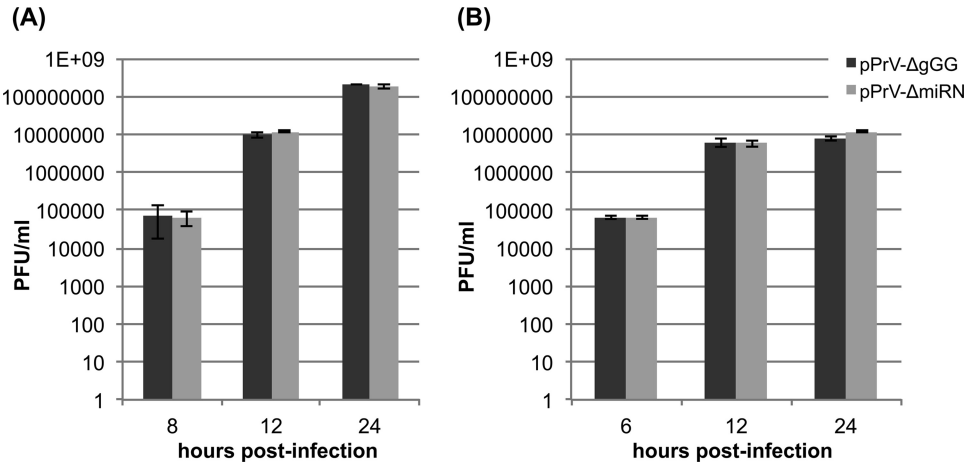

FIG 2 Replication of pPrV-ΔgGG and pPrV-ΔmiRN in PK15 (A) and RK13 (B) cells. Progeny virus titers were determined between 4 and 24 h after infection at a multiplicity of infection (MOI) of 10 (PK15) or 5 (RK13). Titers represent mean values from three independent experiments with bars showing standard deviations.

resulting in pPrV-ΔmiRN (Fig. 1B). The correct insertion of the selection markers and precise deletion of PrV sequences were confirmed by restriction analyses and Southern blot hybridization, as well as by PCR amplification and sequencing of the mutated genome region (results not shown). Infectious PrV was rescued after transfection (FuGene HD reagent; Promega) of rabbit kidney (RK13) cells with BAC DNA.

Propagation, titration, and growth kinetics of pPrV-ΔgGG and pPrV-ΔmiRN. Rabbit (RK13) and porcine (PK15) kidney cells were used for productive virus replication. RK13 cells were grown in minimum essential medium (MEM) supplemented with 10% fetal bovine serum (FBS). For the determination of one-step growth kinetics, cells were infected on ice with pPrV-ΔmiRN or pPrV-ΔgGG at a multiplicity of infection (MOI) of 5 and shifted to 37°C after 1 h. After an additional hour, nonpenetrated virus was inactivated by low-pH treatment (27), and the inoculum was replaced by fresh medium. At different times of culture at 37°C (Fig. 2), the infected cells were lysed by freeze-thawing, and progeny virus titers were determined by plaque assays overlaid with semisolid MEM containing 5% FBS and 6 g/liter methylcellulose. Mean titers from three independent experiments and mean diameters from 30 plaques per virus mutant, as well as standard deviations, were calculated.

PK15 cells were cultivated in Dulbecco's modified Eagle's medium (DMEM) supplemented with 10% FBS, 100 U/ml penicillin, and 100 μg/ml streptomycin at 37°C in the presence of 5% CO_2. PK15 cells were grown in 6-well culture plates. After reaching 90 to 100% confluence, cells were infected with either pPrV-ΔgGG or pPrV-ΔmiRN at an MOI of 10 and incubated for 45 min at room temperature. The inoculum then was aspirated, and cells were washed several times and incubated with DMEM supplemented with 10% FBS. Supernatants and cells were harvested at different times and used (i) for viral titrations and growth kinetics as for RK13 cells (Fig. 2) and (ii) for total RNA extractions, followed by quantitative RT-PCR (RT-qPCR) of viral genes and miRNAs.

Establishment of PrV latency *in vivo*. The *in vivo* animal experiment was approved by an independent ethical committee (7221.3-1.1-016/12). Fifteen 60-day-old pigs (German Landrace) were used for experimental infection. Animals were housed in the biosafety level 3 (BSL3) facility of the Friedrich-Loeffler-Institut, Germany, and tested for the absence of PrV antibodies prior to the start of the experiment. Three groups of five animals each were infected intranasally with 10^5 PFU of pPrV-ΔgGG (animal no. WT 54 to 58) or pPrV-ΔmiRN (animal no. M 49 to 53) or were mock infected (control group; animal no. C 21 to 25). The pigs were allowed to recover during the following 62 days to ensure the establishment of latency. During this time, pigs were monitored for clinical symptoms. In order to check for virus shedding, nasal swabs were collected every 2 days after infection until virus excretion ceased. Blood samples were collected at 4, 7, 10, 15, 20, 30, 45, and 62 days postinfection (p.i.) using a V-trough device.

The host antibody response was assessed by enzyme-linked immunosorbent assay (ELISA) using PrV gB as the antigen. DNA samples from nasal swabs were analyzed by quantitative real-time PCR targeting the gB gene (28).

Animals were slaughtered at 62 days p.i. Trigeminal ganglia were excised, rinsed with ice-cold physiological saline solution, frozen in liquid nitrogen within 30 min after excision, and stored at −80°C until processed.

Nucleic acid extraction and purification. Total RNAs from infected PK15 cells were extracted using QIAzol reagent and purified with an RNeasy minikit according to the manufacturer's instructions (Qiagen).

Frozen trigeminal ganglia were homogenized in ice-cold TRIzol reagent using an Ultra-Turrax (IKA). RNA extraction was performed according to the manufacturer's instructions (Invitrogen). Genomic DNA was obtained upon phase separation for RNA extraction by adding a back extraction buffer containing 4 M guanidine thiocyanate, 50 mM sodium citrate, and 1 M Tris, pH 8.0 (free base), to the interphase-organic-phase mixture. After centrifugation at 12,000 × *g* for 15 min at 4°C, the upper aqueous phase containing DNA was transferred to a clean tube and DNA was precipitated by adding 0.8 volumes of isopropanol per 1 ml of TRIzol, followed by centrifugation at 12,000 × *g* for 5 min at 4°C and pellet washing with 75% ethanol.

Yields and purity of nucleic acids were measured with a NanoDrop ND-1000 spectrophotometer. To remove unwanted residual DNA, all RNA samples were treated with TURBO DNase (Ambion). PK15 RNAs were treated with DNase twice and further checked by qPCR of viral genes to ensure the complete removal of PrV genomic DNA. RNA integrity was assessed using an Agilent 2100 Bioanalyzer and RNA 6000 Nano kits (Agilent), and the RNA integrity number (RIN) (29) was calculated.

Estimation of relative amounts of PrV genomes in trigeminal ganglia. The relative amount of PrV genomes in trigeminal ganglia was estimated by a classical qPCR approach (30). DNA was extracted from a single whole ganglion per animal and amplified using primers specific to the GFP gene (forward primer, GCA AAG ACC CCA ACG AGA AG; reverse primer, TCA CGA ACT CCA GCA GGA CC). For each biological sample, three technical replicates were run, and all qPCRs were performed on the same run to minimize interexperimental variation. Triplicate reaction mixtures (20 μl) included 5 μl genomic DNA (corresponding to 100 ng of DNA), 10 μl of SYBR green PCR master mix, and 5 μl of primers (300 nM each). Reaction mixtures were incubated in a 96-well optical

plate at 95°C for 10 min, followed by 40 cycles at 95°C for 15 s and 60°C for 1 min using a 7900HT Fast real-time PCR system instrument (Applied Biosystems). To avoid false-positive results, the DNA of three negative controls was used (samples 22 C, 23 C, and 25 C). The PrV genome copy number was estimated per 100 ng of genomic DNA from a PA-GFP-coilin C2 plasmid DNA standard curve.

RNA-seq and small RNA-seq library preparation and sequencing. Both RNA sequencing (RNA-seq) and small RNA-seq libraries were prepared and barcoded using the TruSeq RNA sample preparation kits and protocols of Illumina.

RNA-seq. For RNA-seq, libraries were prepared from nine individual samples: three control (C) ganglia, three ganglia latent for pPrV-ΔgGG (WT ganglia), and three ganglia latent for pPrV-ΔmiRNA (M ganglia). Poly(A)-RNA was purified from total RNA using oligo(dT) magnetic beads, fragmented, and reverse transcribed using random primers. Libraries were checked with the Agilent high-sensitivity DNA kit and quantified with the qPCR NGS library quantification kit (Agilent). The nine tagged cDNA libraries were pooled, quantitated by qPCR, and sequenced in paired-end mode (100-bp reads) on an Illumina HiSeq2000 instrument (TruSeq PE cluster, v3; TruSeq SBS, 200 cycles, v3; and TruSeq multiplex primer kit). Quality control analysis of the raw data set did not indicate any differences among lanes regarding the quality or quantity of the reads generated.

Small RNA-seq. Small RNA-seq libraries were prepared for three control ganglia, five ganglia latent for pPrV-ΔgGG (WT-ganglia), and five ganglia latent for pPrV-ΔmiRNA (M-ganglia). Prior to library preparation, the integrity of the RNAs was assessed using an Agilent 2100 Bioanalyzer, and yields were estimated with a Qubit fluorometer. RNAs were fractionated in a 15% denaturing polyacrylamide gel. Small RNA fragments in the range of 18 to 30 nt were excised from the gel and purified. The 5′ and 3′ termini of the small RNAs were ligated sequentially with adapters, followed by reverse transcription and PCR amplification. The amplified cDNA products pooled were sequenced in single-end mode (50-bp reads) using the TrueSeq SBS kit, v3, according to the manufacturer's instructions on a HiSeq1000 Illumina sequencer. Raw reads were analyzed with Casava1.8.2.

Deep sequencing and differential expression analysis. (i) RNA-seq. First, 3′-end reads were trimmed for low-quality bases. Briefly, the 3′-end bases were sequentially cut off if their Phred quality score was below 10 or until the read length became less than 40 bp long. Trimmed reads then were mapped against the *Sus scrofa* reference genome sequence, v10.2 (31), using TopHat, v2.0.4 (32). A transcript annotation was downloaded from Ensembl (v.67) (www.ensembl.org) and supplied to TopHat with option-g. Transcript assembly was performed by providing mapped reads to Cufflinks v2.1.1 (33), and option -g was used to report all reference transcripts as well as any novel genes and isoforms that were assembled. Transcript quantification was performed using HTSeq-count (from the HTSeq framework, version 0.5.4p3) in default (union) mode, and these counts were used to perform differential expression analysis. Normalization and a generalized linear model (GLM) likelihood ratio test were performed using the Bioconductor edgeR package (version 3.2.3) (34) in the R environment (version 3.0.0). Transcripts showing a Benjamin-Hochberg false discovery rate (FDR) below 0.05 were considered differentially expressed.

(ii) Small RNA-seq. Raw reads first were trimmed for adapters and low-quality ends (cutoff Phred quality score, 20) using cutadapt v.1.3 (35). Scripts from the miRDeep2 (v.2.0.0.5) software package (36) then were used for the identification and quantification of novel and known miRNAs from the trimmed reads. Mapping against the pig genome reference sequence (*Sus scrofa* v10.2) was performed with the script mapper.pl, while the identification of known and novel miRNAs was done using miRDeep2.pl script. The known and predicted miRNAs then were provided to the quantifier.pl script. This module maps the deep-sequencing reads to predefined miRNA precursors. These signatures then were post-processed using a custom python script to quantify mature miRNAs. To discard hairpins with a read distribution inconsistent with Drosha and Dicer processing sites (i.e., reads tilled across the precursor), we expected at least a 3:1 ratio between reads that matched any of the stem-loop arms and reads located in the loop. For the remaining hairpins, reads that mapped inside the loop (more than 3 nucleotides falling in the loop) were not considered for quantification. When no known mature miRNA matched the same precursor, putative new mature miRNAs were named based on the name of the hairpin on which they were located or from the name of the known miRNA mapping on the opposite strand of the precursor. All of the reference sequences from mature miRNAs and their precursors were obtained from the miRBase database, v20 (www.mirbase.org) (37). These counts were used to perform differential expression analysis. Normalization and a GLM likelihood ratio test were performed using the Bioconductor edgeR package (version 3.2.3) (34) in the R environment (version 3.0.0). The miRNAs showing a Benjamin-Hochberg FDR below 0.05 were considered differentially expressed.

RT-qPCR analyses. (i) Porcine and viral genes. To validate the RNA-seq data of trigeminal ganglia, 16 genes were selected to represent most of the predicted PrV miRNA targets (see below) and a wide abundance range in ganglia (number of RNA-seq reads). A second set of genes included the viral genes LLT, EP0, IE180, US1, US3, US7, US8, UL6, UL28, UL32, UL33, UL43, UL47, and UL48. With the exception of primers for LLT, all primers for PrV genes have been reported (38). Primers for LLT and for all porcine genes were designed using Primer3Plus software (39) and verified for specificity by BLAST analysis (see Table S1 in the supplemental material).

Reverse transcription was performed with the SuperScript III first-strand synthesis system (Invitrogen) using between 800 ng and 1 μg of total RNA and 50 ng of random hexamers. The quantity and quality of cDNAs were evaluated using an Agilent 2100 Bioanalyzer and RNA 6000 Pico kits (Agilent). All RT-qPCRs were performed on a 7900HT fast real-time PCR system instrument (Applied Biosystems) using the SYBR green PCR master mix. For each primer pair, PCR efficiency was evaluated using serial dilutions of cDNA sample. The potential occurrence of dimers and amplification specificity was assessed by melting curve analyses. An equivalent of 500 pg of cDNA was used as the template for each sample, and three technical replicates were run as previously described (see "Estimation of relative amounts of PrV genomes in trigeminal ganglia"). A parametric two-tailed Student's *t* test was used to assess statistical differences between pairwise comparisons.

(ii) PrV miRNAs. Stem-loop RT primers, PCR primers, and probes were optimized for improved stability and mismatch discrimination using locked nucleic acid nucleotides (40, 41) (see Table S1 in the supplemental material).

Reverse transcription was done using the TaqMan microRNA reverse transcription kit (Applied Biosystems). In each reaction mixture, 10 ng of total RNA from trigeminal ganglia/PK15 cells was mixed with 50 nM specific stem-loop RT primer. RT reactions were carried out at 16°C for 30 min, 42°C for 30 min, and 85°C for 5 min. The qPCRs were made using standard TaqMan PCR protocols on a 7900HT fast real-time PCR system instrument (Applied Biosystems).

Target gene predictions of PrV miRNAs. The target sites of all PrV miRNAs on differentially expressed genes (see Table S3 in the supplemental material) were predicted by TargetScan 6.0 (42, 43). As few genes had annotated 3′-untranslated regions (UTRs), we first manually annotated as many missing genes as possible, making use of cross-species mRNAs where pig-specific sequences were unavailable (44). This annotation is available from the Vega website (http://vega.sanger.ac.uk).

Predictions could be computed on 34 out of the 54 differentially expressed genes (see Table S3 in the supplemental material). The 3′UTR sequences from the EPO (Enredo, Pecan, Ortheus) pipeline for 12 eutherian mammal species multiple alignments were retrieved from Ensembl v.68 (www.ensembl.org). Genes having a target site context score equal to or greater than zero were filtered out of the analysis. An enrichment analysis was carried out to check if differentially expressed genes were enriched

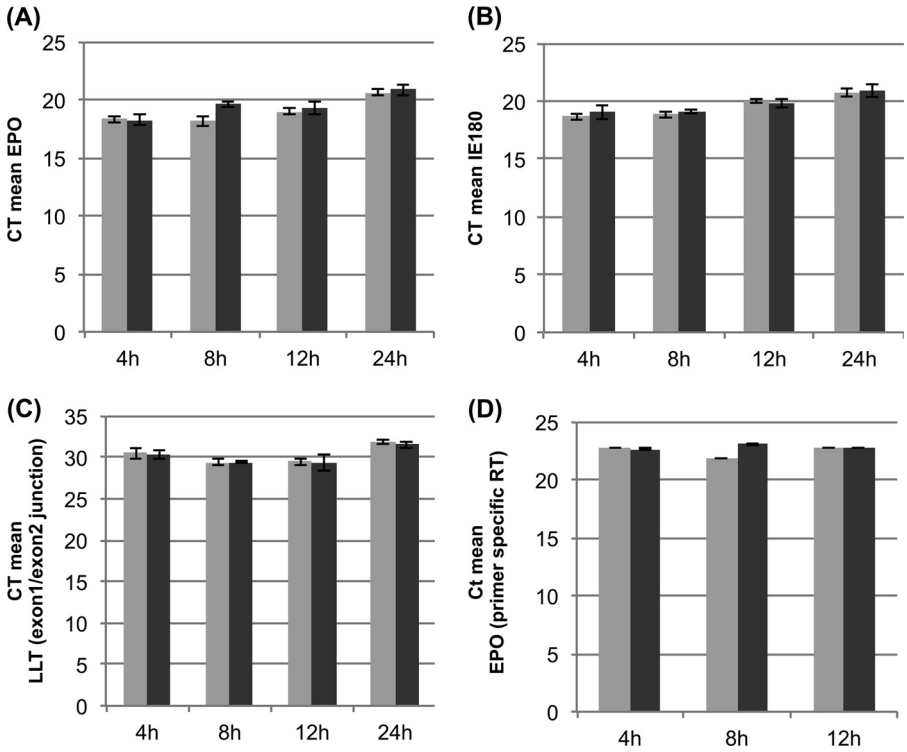

FIG 3 RT-qPCR expression kinetics of EP0 (A and D [after primer-specific RT]), IE180 (B), and the LLT exon1/exon2 junction (C) during PrV infection *in vitro*. PK15 cells were infected with pPrV-ΔmiRN (light gray) and pPrV-ΔgGG (dark gray) at an MOI of 10. Values are provided as mean C_T values and are the averages from three biological replicates (higher C_T values mean decreased gene expression levels). The qPCRs were normalized to the input amount of total RNA.

in miRNA targets compared to the number of targets predicted on the total number of genes expressed in ganglia using Fisher's exact test.

Gene pathway analysis. The Ingenuity Pathways Analysis (IPA) software was used to identify the most relevant biological functions and pathways involving the genes found differentially expressed in pairwise comparisons between WT, M, and C ganglia. We first uploaded the list of human homologs that corresponded to the pig genes into the application. The network analysis in the WT versus C and M versus C data sets aimed to search both direct and indirect interactions (known from the literature) between differentiated genes and all other molecules (genes, gene products, or small molecules) contained in the Ingenuity Knowledge Base (IKB). For a given network, the degree of association is estimated by considering the proportion of eligible genes (genes with at least one interaction with another full-length gene or protein in IKB), and a score is assigned based on the right-tailed Fisher exact test [log(1/*P* value)]. The IPA upstream regulator analysis was used to identify upstream regulators and predict, based on the literature compiled in the IKB, whether they are activated or inhibited given the observed gene expression changes in the WT versus C and M versus C data sets. The activation *z* score predicts the activation state of the upstream regulator using the gene expression patterns of the genes downstream of an upstream regulator; an absolute *z* score of ≥2 is considered significant. Finally, the heatmap comparison analysis tool was used to visualize clusters of diseases and biofunctions predicted to increase or decrease similarly across the WT versus M and M versus C data sets. The statistical significance of each biofunction is expressed as *P* values from Fisher's exact test, and a total absolute *z* score across all of the observations is provided.

RNA-seq accession numbers. The raw reads determined in this work have been deposited at the European Nucleotide Archive (ENA) under accession number PRJEB6754 for RNA-seq (http://www.ebi.ac.uk/ena/data/view/PRJEB6754) and accession number PRJEB6755 for small RNA-seq (http://www.ebi.ac.uk/ena/data/view/PRJEB6755).

RESULTS

Generation and *in vitro* characterization of a PrV miRNA mutant. pPrV-ΔmiRN was generated from the parental pPrV-ΔgGG (Fig. 1A) (24) by deleting nucleotides 98100 to 100570 from the right end of the U_L region of the PrV-Ka genome (GenBank accession no. JQ809328) (26). The deletion includes 9 out of the 11 described miRNA genes (22, 23) but excludes the two miRNA genes transcribed from the inverted repeat sequences (prv-miR-LLT10 and prv-miR-LLT11) (Fig. 1B).

The deletion is completely located within the intron of the LLT (8) without affecting the predicted splice donor, branch, or acceptor sites. Due to the insertion of the bacterial genes (Fig. 1B), the genome size of pPrV-ΔmiRN is reduced by only 1,154 bp compared to pPrV-ΔgGG, which is unlikely to significantly influence the efficiency of viral DNA replication or packaging. Consistently, pPrV-ΔmiRN and pPrV-ΔgGG exhibited almost identical *in vitro* replication properties with respect to replication kinetics (Fig. 2) and cell-to-cell spread in RK13 and PK15 cells (data not shown).

The expression of the genes adjacent to the deletion (IE180 and EP0) was profiled by RT-qPCR in PK15 cells. In cells infected with pPrV-ΔmiRN, EP0 was transiently overexpressed, peaking at 8 h p.i. (Fig. 3A and D), while IE180 and the spliced LLT product (exon 1-exon 2 [ex1/ex2] junction of LLT) displayed very similar profiles of expression in cells infected with either pPrV-ΔmiRN or pPrV-ΔgGG (Fig. 3B and C). Similar expression profiles were found for 11 other PrV genes (not shown). Thus, as desired, mutant and wild-type PrV displayed highly similar *in vitro* properties as an essential prerequisite for the following *in vivo* studies.

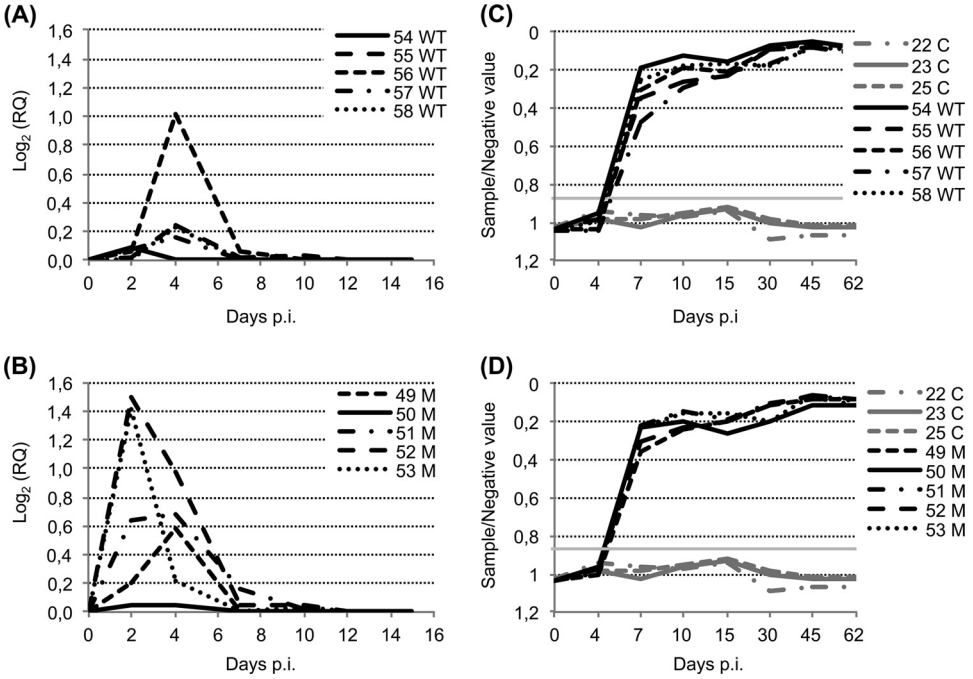

FIG 4 Establishment of latency *in vivo*. Pigs were infected with either pPrV-ΔgGG (WT 54 to 58) or pPrV-ΔmiRN (M 49 to 53) or were mock infected (C 22 to 25). (A and B) DNAs from nasal swabs of animals infected by WT PrV (A) or M PrV (B) were analyzed by RT-qPCR of the PrV gB gene $\log_2$ (RQ), $\log_2$ of relative quantity. (C and D) The host antibody response was analyzed by ELISA using PrV gB as the antigen. The threshold value of the assay (0.7) is indicated as a horizontal line.

Both pPrV-ΔmiRN and pPrV-ΔgGG establish latency *in vivo*. Groups of five animals were infected with pPrV-ΔgGG (WT) or pPrV-ΔmiRN (M) or were mock infected (C). The only clinical symptom detected was intermittent fever until 5 days p.i. All infected animals recovered, while two noninfected control animals died in the course of the experiment due to stress reaction.

The levels of virus excretion in nasal swabs were heterogeneous. On average, the animals infected by M showed higher excretion levels than those infected by the WT, with maximum levels reached earlier (at 2 days p.i.) in two of the M-infected animals. No virus excretion was detected in nasal swabs from 12 days p.i. (Fig. 4A and B). All infected animals developed a robust immune response with no differences between M and WT infection (Fig. 4C and D).

Animals were sacrificed at day 62 p.i. PrV genomes were detected in the trigeminal ganglia (WT ganglia and M ganglia) of all infected animals. Values ranged between 57 and 542 copies per 100 ng of genomic DNA, which is similar to the range found in previous studies on herpes simplex virus (HSV) (45). Some of the highest values were found in M ganglia (Fig. 5). This showed that the deletion did not impair the mutant virus in access to and establishing latency in trigeminal ganglia.

Descriptive statistics of small RNA-seq and RNA-seq of trigeminal ganglia. We generated individual libraries and profiled,

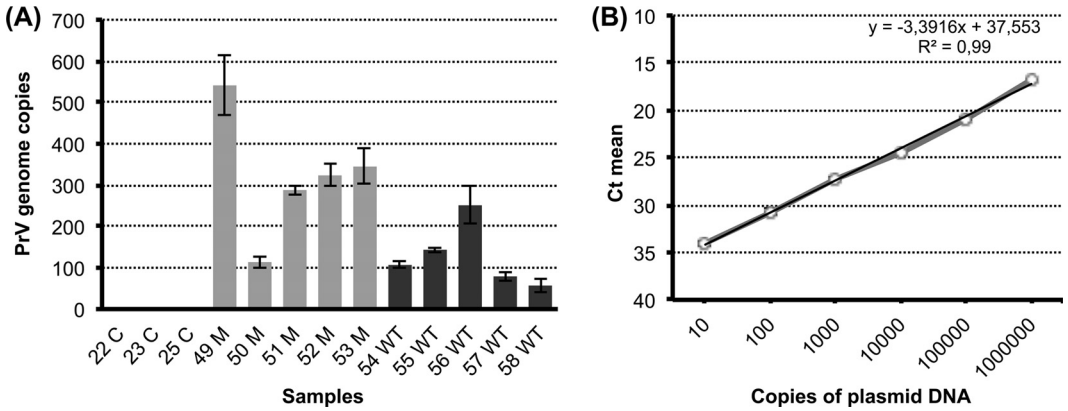

FIG 5 Relative amounts of PrV genomes in latent trigeminal ganglia. (A) The PrV genome copy value per 100 ng of genomic DNA was quantified by qPCR using a GFP amplicon. (B) PA-GFP-coilin C2 plasmid DNA standard curve. The *x* axis represents the input copies of plasmid DNA, and the *y* axis represents the mean threshold cycle (C_T mean).

TABLE 1 Descriptive statistics of small RNA profiling of porcine trigeminal ganglia latent for either the WT or M PrV[a]

Sample	No. of reads mapping on miRNAs	No. of reads <16 nt and >29 nt	Total no. of reads
22 C	7.8	16.9	42.9
23 C	5.8	8.7	46.8
25 C	7.2	12.9	27.3
49 M	6.9	14.8	55.3
50 M	20.7	34.7	47.9
51 M	11.3	17.7	43.8
52 M	16	15.9	46.1
53 M	16.3	19.8	39.2
54 WT	10	8	20.7
55 WT	5.7	16.5	27.4
56 WT	25.6	32.8	46.5
57 WT	15	19	20.7
58 WT	13.5	15.9	28.4
Avg counts	12.4 ± 6.1	18.0 ± 7.8	37.9 ± 11.5

[a] Thirteen individual small RNA-seq libraries were constructed from five WT-infected animals (54 WT, 55 WT, 56 WT, 57 WT, and 58 WT), five M-infected animals (49 M, 50 M, 51 M, 52 M, and 53 M), and three mock-infected animals (22 C, 23 C, and 25 C). Values are indicated as millions of normalized reads. The average counts are provided at the bottom of each column.

by small RNA-seq, the ganglia derived from all 13 surviving animals. The sequencing depth ranged from 20.7 to 47.9 million reads with a mean depth of 37.9 million reads per sample. After adapter trimming and filtering out low-quality reads, porcine and PrV miRNAs were identified and mapped on the pig and PrV genomes. This led to the identification of between 5.8 and 20.7 million reads per library mapping to known or novel miRNAs (Table 1).

The vast majority of sequences recovered proved, as expected, to be porcine cellular miRNAs. The most highly expressed miRNAs were ssc-miR-27b-3p and ssc-miR-143-3p, with average read counts of about 2 and 1 million, respectively. Further analysis did not provide any significant evidence of host miRNAs differentially expressed in the pairwise comparisons among M, WT, and C ganglia. Differences were observed for ssc-miR-204 expression between WT and C ganglia and for ssc-miR-429 expression between M and WT ganglia. However, after manual checking of reads, these turned out to be artifacts due to the abnormally high number of reads in outlier samples, specifically of ssc-miR-204 in one C ganglion sample and of ssc-miR-429 in one M ganglion sample (data not shown).

RNA-seq. We produced individual libraries for a sample of nine animals (3 M, 3 WT, and 3 C ganglia). RNA-seq profiling generated an average of 65 million reads per library. A quality check confirmed that over 75% of reads were of good quality. Upon mapping and transcript assembly, we detected 19,465 pig genes expressed in ganglia. Normalized values are provided in Table S2 in the supplemental material. The most expressed pig genes (average of 700,000 reads per sample) corresponded to the neurofilament medium and light polypeptide genes (NEFM and NEFL), which are highly expressed in the cerebral cortex and in the hippocampus (46, 47). Despite the depth of sequencing, very few reads mapped to the PrV genome (between 51 and 523 normalized reads). All of them mapped to the LLT gene locus during latency, as expected (see Table S2 in the supplemental material).

All known PrV miRNAs are expressed during latency. In the ganglia latent for parental PrV (WT ganglia), we detected all of the mature PrV miRNAs described so far, which are encoded by 11 miRNA genes clustering in the LLT intron (22, 23). No new PrV miRNAs were identified (Table 2). Furthermore, we did not detect the offset-miRNA (moRNA) encoded by the prv-mir-LLT8 gene previously found in dendritic cells during productive PrV infection, identified as prv-miR-4 (22) or moR-8 (23, 48).

The PrV miRNAs still are annotated as unique mature sequence in the latest version (v21) of the miRBase database (www.mirbase.org). However, with few exceptions, all miRNAs were found expressed by both the 5′ and 3′ arms of their precursor sequences, and as expected, one form was predominant (Table 2). Furthermore, the predominant mature miRNAs encoded by the prv-mir-LLT7 and prv-mir-LLT8 genes were those of the 3′ arm, as previously detected (23, 48) but not yet annotated in miRBase. To clarify the issue, we revised the nomenclature of all PrV miRNAs by adding the arm of origin information (Table 2).

The most abundant viral miRNA was prv-miR-LLT2-5p, followed by prv-miR-LLT1-3p (both deleted in M) and prv-miR-LLT-10-3p (present in both WT and M) (Table 2). The prv-mir-LLT-10a and prv-miR-LLT-11a genes map to the 3′ distal portion of the LLT intron and are duplicated in the terminal repeat region (TR) of the PrV genome (prv-mir-LLT10b and prv-mir-LLT11b). The mature prv-miR-LLT-10 and prv-miR-LLT-11 showed similar patterns of expression in M and WT ganglia, suggesting that the deletion in the mutant virus did not affect regulatory sequences required for the expression of prv-mir-LLT10a and prv-mir-LLT11a (Table 2).

The RT-qPCRs confirmed the presence of the three most abundant miRNAs (prv-miR-LLT1-3p, prv-miR-LLT2-5p, and prv-miR-LLT-10-3p) (Fig. 6A). For comparison, we checked the expression of these miRNAs in PK15 cells during productive infection at 12 h p.i. Both prv-miR-LLT1-3p and prv-miR-LLT2-5p were highly expressed, while prv-miR-LLT-10-3p was detected at much lower levels (Fig. 6B). We were unable to assess the expression levels of other less abundant PrV miRNAs above background values.

Characterization of the pattern of expression of the LAT locus in trigeminal ganglia. RNA-seq and small RNA-seq data indicated that only LLT and the viral miRNAs (which, with the exception of prv-miR-LLT10 and prv-miR-LLT11, are present only in the genome of WT) were expressed in the porcine ganglia, as would be expected in established latency. To better characterize this status in the M ganglia, we performed RT-PCR and RT-qPCR analyses of different portions of the LAT locus adjacent to the deletion (Fig. 1).

In both M and WT ganglia, no expression of IE180 or EP0 could be detected by repeated tests with primer-specific RT-qPCR. This confirmed that also the second copy of the IE180 gene mapping to the TR region of the PrV genome (1) is inactive during latency. The M virus expressed lower levels of transcripts comprising the ex1/ex2 junction and exon 2 of LLT, while the first LLT exon was expressed at similar levels by both viruses (Fig. 7). This was surprising, given that the splicing of LLT (LLT ex1/ex2 junction) was unaffected *in vitro* (Fig. 3C) and no expression of genes expressed during the lytic phase was detected in ganglia.

An additional difference was observed in the distribution of RNA-seq reads between M and WT ganglia at the LAT locus. This revealed that in M ganglia, the portion of the LLT intron ~1,000 bp immediately downstream of the deletion is expressed (Fig. 8).

TABLE 2 Expression levels of PrV miRNAs in trigeminal ganglia latent for the WT or M PrV[a]

miRNA name	miRBase ID	miRBase accession no.	Mature miRNA sequence (5′–3′)	Expression level of[b]: WT 54	WT 55	WT 56	WT 57	WT 58	M 49	M 50	M 51	M 52	M 53
prv-mir-LLT1-5p			GACGGCTCCTGGGGCTGAAAGC	0.18	0.60	1.84	0.27	0.15					
prv-mir-LLT1-3p	**prv-miR-LLT1**	**MIMAT0025304**	UCUCACCCCUGGGUCCGUCGC	25.11	43.27	76.90	5.54	17.18					
prv-mir-LLT2-5p	**prv-miR-LLT2**	**MIMAT0025305**	CUCAUCCCGUCAGACCUGCG	55.17	344.02	153.63	14.34	35.02					
prv-mir-LLT2-3p			CGCGGGGCAACGGTGGTGAG	0.35		0.31	0.13	0.07					
prv-mir-LLT3-5p			GAGCCGGGGGGGTCGAGTG										
prv-mir-LLT3-3p	**prv-miR-LLT3**	**MIMAT0025306**	CGCACACGCCCCUCUCGCGCAC	0.18	0.70	1.80		0.37					
prv-mir-LLT4-5p	**prv-miR-LLT4**	**MIMAT0025307**	AGAGUAUCAGCGUGGCUUUUUU	4.42	4.59	23.07	1.40	2.59					
prv-mir-LLT4-3p			AAAAGGCACGCTGATGCGTCC			0.12							
prv-mir-LLT5-5p													
prv-mir-LLT5-3p	**prv-miR-LLT5**	**MIMAT0025308**	UGAGUGGAUGGAUGGAGGCGAG		0.50	1.21	0.20						
prv-mir-LLT6-5p	**prv-miR-LLT6**	**MIMAT0025309**	CGUACCGACCCGCCUACCAGG		3.39	1.02							
prv-mir-LLT6-3p			CTTGGCAGCGGGTGGGTACC		0.80	0.70	0.07	0.22					
prv-mir-LLT7-5p	**prv-miR-LLT7**	**MIMAT0025310**	CCGGGGGGUUGAUGGGGAU										
prv-mir-LLT7-3p			ACCACCGTCCCCCTGTCCCT	1.42	4.29	5.70	2.27	2.00					
prv-mir-LLT8-5p	**prv-miR-LLT8**	**MIMAT0025311**	GUGGGGGCGAAGAUUGGGUU			1.84	0.07						
prv-mir-LLT8-3p			CAACCCTTCTGGAGCCCTACC	10.79	8.57	30.25	2.27	5.48					
prv-mir-LLT9-5p	**prv-miR-LLT9**	**MIMAT0025312**	AUCGAGGAGAUGUGGAGGGG		0.20	0.59		0.07					
prv-mir-LLT9-3p			CCCTCCCCCGCATCTCTTCTC			0.43	0.13						
prv-mir-LLT10b-5p									0.15				
prv-mir-LLT10b-3p	prv-miR-LLT10a, prv-miR-LLT10b	MIMAT0025313, MIMAT0025314	CCGAGCCUGCCCCUUCCGUCGCA	24.05	51.74	74.05	4.47	10.51	18.93	4.68	11.13	17.36	75.16
prv-mir-LLT11b-5p	prv-miR-LLT11a, prv-miR-LLT11b	MIMAT0025315, MIMAT0025316	AGGCUGGGAGUGGGGACGGAAGA	0.18		1.02	0.13					0.08	0.37
prv-mir-LLT11b-3p					0.80	1.17	0.07	0.07		0.05			0.25

[a] Names, identifiers (ID), and accession numbers in boldface indicate miRNAs deleted from the M genome. Both prv-mir-LLT10 and prv-mir-LLT11 are duplicated in the PrV genome as identical genes (prv-mir-LLT10a and prv-mir-LLT10b as well as prv-mir-LLT11a and prv-mir-LLT11b).

[b] Values are provided as counts per million reads (cpm).

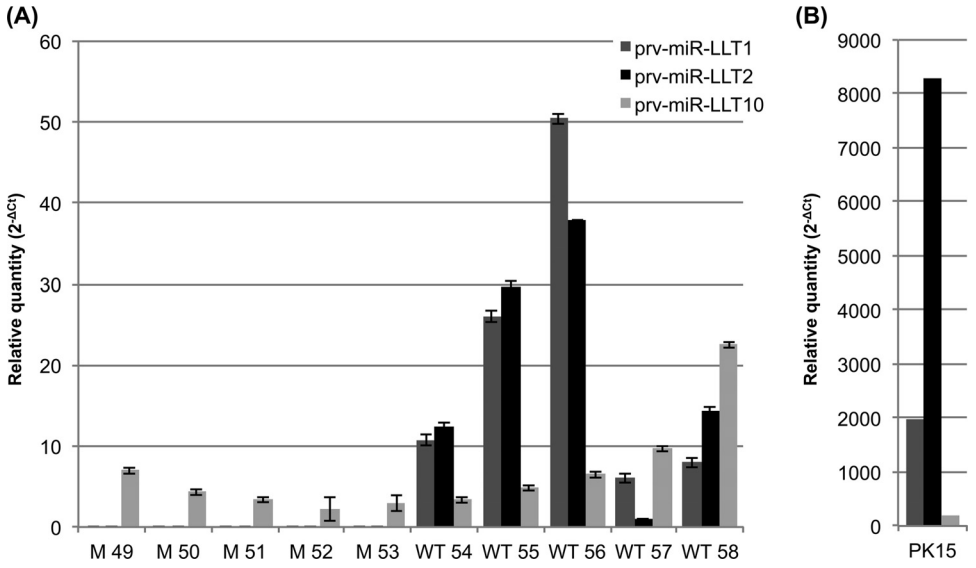

FIG 6 RT-qPCR profiles of prv-miR-LLT1, prv-miR-LLT2, and prv-miR-LLT10 in trigeminal ganglia latent for the WT or M PrV (A) and in PK15 cells at 12 h p.i. with the WT PrV (B). Values are normalized against the background and are indicated as $2^{-\Delta CT}$(± standard deviations).

We tested by RT-qPCR if this indicated the presence in M ganglia of unspliced transcripts which are expressed during the PrV lytic phase (12). The results confirmed that the bacterial genes and the LLT intron region immediately downstream of the bacterial cassette (Fig. 1) were expressed by the M virus, indicating that the bacterial promoter is active in ganglia. However, in agreement with the distribution of mapped reads, no expression of the portion of the LLT intron adjacent to the acceptor site and preceding the peak of reads at the 5′ of LLT exon 2 was detected by RT-qPCR in M and WT ganglia (not shown). This excluded the possibility that transcripts covering part of the 3′ portion of the intron are expressed in M ganglia.

Gene upregulation is prevalent in trigeminal ganglia latent for the mutant PrV. By differential expression analysis of the nine samples profiled by RNA-seq, we identified 54 genes (plus two pseudogenes and two miRNA precursors predicted in the cow genome), each significantly differentially expressed (DE) in at least one of three pairwise comparisons among WT, M, and C ganglia (WT versus C, M versus C, and M versus WT). Values of differential expression (DE and *P* values of significance) are provided in Table S3 in the supplemental material.

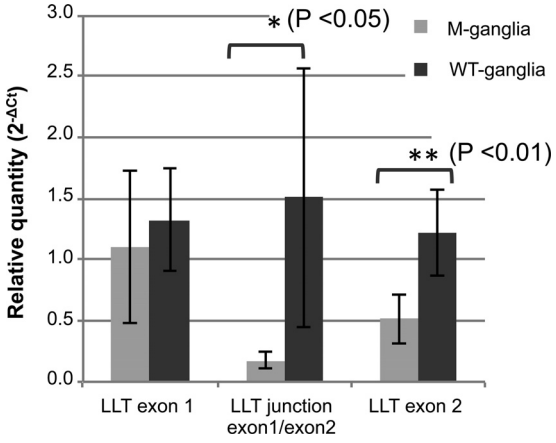

FIG 7 Pattern of transcription of three regions of LLT (exon 1, ex1/ex2 junction, and exon 2) in trigeminal ganglia latent for WT or M PrV. RT-qPCR values were calibrated versus the relative amounts of PrV genomes. Data are $2^{-\Delta CT}$ (± standard deviations) values calculated from three technical replicates.

M ganglia and WT ganglia differed considerably in their patterns of gene expression. DE genes reaching significance were more abundant in WT (34 genes) than in M ganglia (22 genes), and only eight genes were common to the M versus C and WT versus C comparison. An additional six genes were significantly DE only in the direct comparison between WT versus M.

Remarkably, while in the WT ganglia we found a prevalence of significantly downregulated genes (20 downregulated versus 14 upregulated), the opposite trend was found in M ganglia (19 upregulated versus only 3 downregulated) (see Table S3 in the supplemental material). Only BTNL9 (butyrophilin-like 9), MTNR1B (melatonin receptor 1B), NR1D2 (nuclear receptor subfamily 1, group D, member 2, which is a transcriptional repressor with roles in circadian rhythms and carbohydrate and lipid metabolism), and MAPK4 (mitogen-activated protein kinase 4) were more significantly downregulated in M ganglia compared to WT ganglia or controls.

The eight genes shared by the M versus C and WT versus C comparisons included only highly upregulated host immune genes: CXCL13 (a chemokine ligand), five immunoglobulins (IgJ, IgK-V, IGKV1D-42, one IGLC member, and IGLL5), TNFRSF10B (member 10B of the tumor necrosis factor [TNF] receptor superfamily, the most upregulated gene found in both M and WT ganglia [>4 logFC, where FC indicates fold change]), and a protein annotated as novel in the pig genome and similar to SLC2A7, which is a glucose transporter (see Table S3 in the supplemental material).

RT-qPCR of 16 genes represented by either a high or low number of RNA-seq reads was carried out in the whole set of WT, M, and C ganglion samples. The results showed excellent concordance between RNA-seq and RT-qPCR. Furthermore, the profile

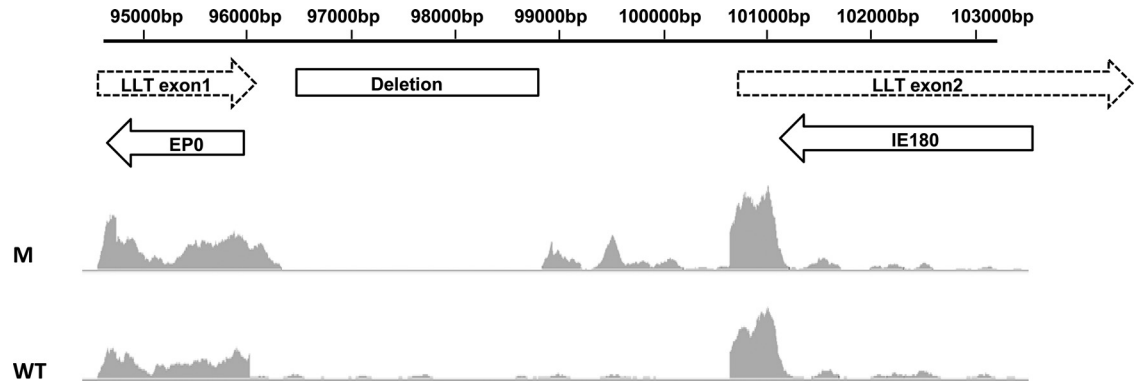

FIG 8 Visualization of the distribution of RNA-seq reads obtained by RNA-seq profiling of trigeminal ganglia latent for the mutant (M) or parental (WT) PrV on the PrV genome.

of these few additional animals provided significance to previously suggestive values (Table 3; also see Table S3 in the supplemental material). In particular, PLA2G2D (phospholipase A2, group IID), CD8A (T-cell surface glycoprotein CD8 alpha chain), and CXCL9 became significant in the M versus WT contrast, strengthening the pattern of gene upregulation found in M ganglia. Furthermore, RT-qPCR confirmed that VIP (vasointestinal peptide) was detectable only in the three M ganglia samples carrying the highest numbers of copies of PrV genomes (Fig. 5).

Fifteen DE genes harbored one or multiple targets for one or more of PrV's miRNAs (see Table S3 in the supplemental material). However, the generalized pattern of gene downregulation in WT ganglia and of gene upregulation in M ganglia hid any putative modulatory effect of PrV miRNAs. Furthermore, we did not detect any relative enrichment of putative targets for the most expressed PrV miRNAs compared to the whole set of porcine genes expressed in ganglia (not shown).

LAT deletion affects the host proinflammatory response. We used the IPA software to analyze the expression patterns of latently infected ganglia. All of the genes which were DE in at least one of the three comparisons (see Table S3 in the supplemental material) were included in the analysis, with the exception of the two putative miRNA precursors so far annotated only in the cow genome (bta-mir-2887 and bta-miR-2904) and C3 (missing from the IPA reference database). By this analysis we could assign a total of 44 of these DE genes to top gene networks and/or biofunctions.

The top network identified by IPA in both M and WT ganglia was termed cell-mediated immune response, cellular movement, hematological system development and function (17 genes; score, 39), followed by hereditary disorder, neurological disease, psychological disorders (15 genes; score, 34) (see Table S4 in the supplemental material). Other networks were identified by fewer than six genes in either the WT versus C or M versus C comparisons.

IPA identified gamma interferon and two inflammatory cytokines (TNF and interleukin-6 [IL-6]) as the most significant top upstream regulators. The state of activation of these regulators was

TABLE 3 Comparison of RNA-seq and RT-qPCR data of 16 genes differentially expressed in trigeminal ganglia latent for the WT or M PrV[a]

Ensembl accession no.	Gene abbreviation	Gene name or description	WT vs C		M vs C		M vs WT	
			RNA-seq	RT-qPCR	RNA-seq	RT-qPCR	RNA-seq	RT-qPCR
ENSSSCG00000028488	LTC4S	Leukotriene C(4) synthase	−1.38*	−0.23	−0.72	−0.76	0.66	0.52
ENSSSCG00000013022	PYGM	Phosphorylase	−1.46*	−0.88	−0.33	0.32	1.13	1.20**
ENSSSCG00000010506	OPALIN	Opalin (specifically expressed in brain)	−3.11*	−3.06	−0.67	−0.40	2.44	2.66*
ENSSSCG00000025434	CGA	Glycoprotein hormones alpha chain	−3.13*	−2.27*	−0.38	−0.72	2.75	1.55*
ENSSSCG00000016664	NPSR1	Member of G protein-coupled receptor 1 family	−2.66*	−0.27	−2.26	0.58	0.40	0.85
ENSSSCG00000003345	TMEM88B	Transmembrane protein 88B	−1.98*	−1.29*	−0.84	0.01	1.14	1.31**
ENSSSCG00000000133	TST	Sulfurtransferase	−0.88*	−0.74	−0.16	−0.02	0.73	0.72*
ENSSSCG00000008648	RSAD2	Viperin antiviral protein	1.36**	1.29	0.62	1.09	−0.73	−0.20
ENSSSCG00000003497	PLA2G2D	Phospholipase A2, group IID	1.30	0.70*	2.25**	1.31*	0.95	0.61
ENSSSCG00000008217	CD8A	T cell surface glycoprotein, CD8 alpha chain	0.50	−0.31	1.37*	1.10*	0.87	1.41**
ENSSSCG00000023489	CXCL9	Chemokine (C-X-C motif) ligand 9	0.81	1.02	1.92***	2.28*	1.12	1.26*
ENSSSCG00000010780	CYP2E1	Cytochrome P450 2E1	−2.28	−1.41	0.78	0.81	3.06*	2.23**
ENSSSCG00000025614	PRICKLE4	LIM protein family member	−1.14	−0.15	1.56	0.56*	2.71*	0.71*
ENSSSCG00000004492	SLC14A1	Membrane transporter of urea in erythrocytes	−1.96***	−1.32*	−0.33	0.34	1.63**	1.66**
ENSSSCG00000009672	SCARA5	A ferritin receptor mediating nontransferrin iron delivery	−0.77*	−0.73	0.27	0.16	1.05***	0.89*
ENSSSCG00000004078	VIP	Vasointestinal neuropeptide					5.85**	6.66*

[a] Values are reported as the fold change (logFC) for each of the three pairwise comparisons (WT versus C, M versus C, and M versus WT). VIP was detected in only three M ganglia samples. *, $P \leq 0.05$; **, $P \leq 0.01$; ***, $P \leq 0.001$.

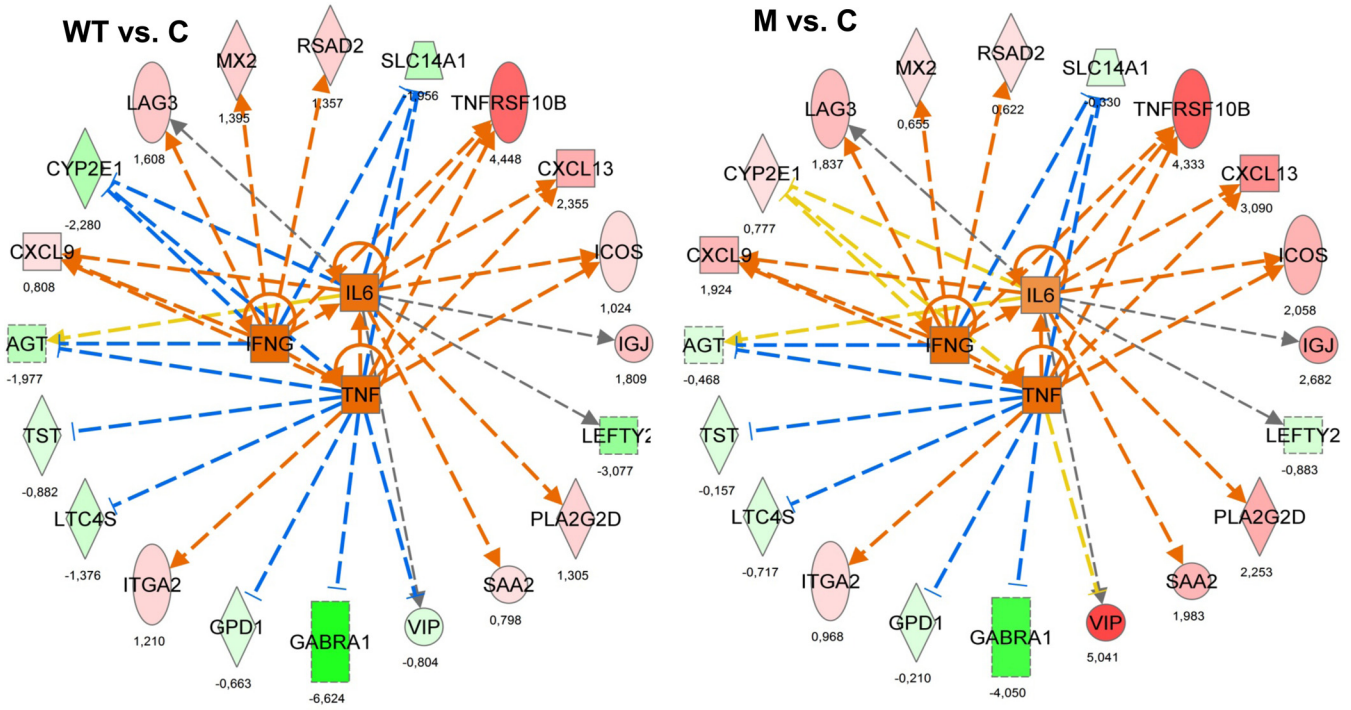

FIG 9 IL-6, gamma interferon, and TNF were identified by IPA as the most significant upstream regulators (*z* scores >2) to explain the pattern of transcription of 20 DE genes, 15 of which belong to the top IPA network, termed cell-mediated immune response, cellular movement, hematological system development, and function (17 DE genes). Left, WT versus C; right, M versus C. Numbers are the logFC values of each comparison. Red, upregulated; green, downregulated; orange, leads to activation; blue, leads to inhibition; yellow, finding inconsistent with state of downstream molecules; gray, effect not predicted.

globally coherent with the pattern of expression of 20 DE genes in the WT versus C and M versus C comparisons (Fig. 9). As expected, the large majority (15 genes) belonged to the cell-mediated immune response network (see Table S4 in the supplemental material). This network added evidence for the pattern of expression of VIP being inconsistent with the activation of TNF, while the pattern of CYP2E1 (cytochrome P450, family 2, subfamily E, polypeptide 1) is inconsistent with all three regulators (Fig. 9).

In order to compare the WT and M ganglia for their respective status of activation of specific diseases and biofunctions, we generated a comparative heatmap of M versus WT ganglia reporting the IPA *z* scores of activation besides the *P* values of the significance of biofunctions (Table 4). The differences in the trend of activation/inhibition between WT and M ganglia are determined largely by a few genes participating in several biofunctions. The migration of dendritic cells was, together with the more general ones related to tissue and cell homeostasis, the most significant biofunction of latent ganglia ($P = 6.77E^{-06}$). Unlike WT ganglia, in M ganglia this biofunction had a trend of inhibition. This difference was due to the combined effect of three genes: VIP (only expressed in M ganglia), AGT (angiotensinogen-serpin peptidase inhibitor, clade A, member 8; less downregulated in M ganglia), and ICOS (inducible T-cell costimulator; more upregulated in M ganglia). A similar effect was found for other biofunctions (activation of leukocytes, activation of T lymphocytes, and inflammatory response). Conversely, the expansion of T lymphocytes and stimulation of cells had a trend of activation in M ganglia due to the combined effect of VIP and BTNL9 (the latter is more downregulated in M ganglia). Interestingly, M ganglia also showed a less efficient inhibition of synthesis of fatty acid and concentration of fatty acid (Table 4).

DISCUSSION

We show here that deletion of nine of the 11 known PrV miRNA genes, contained in a cluster within the LLT intron sequence, does not impair the establishment of latency in trigeminal ganglia. The PrV genome was detected in the trigeminal ganglia of all infected animals beyond the termination of clinical symptoms and viral excretion (Fig. 4 and 5). Moreover, the mutant virus displayed properties almost identical to those of the parental pPrV-ΔgGG, a BAC clone derived from PrV-Ka, during propagation *in vitro* (Fig. 1 to 3).

The value of our experimental approach lies in the use of a natural virus-host system to analyze the importance of miRNA-containing regions on herpesvirus latency. Most of the current knowledge on latency has been obtained from studies of HSV-1 and HSV-2 in rodent models. In these settings, all LAT mutants that ablate LAT expression and the expression of multiple miRNAs can establish and maintain latency (18, 41–43). It was reported earlier that PrV mutants unable to express LAT and EP0 also were able to reach and persist in porcine trigeminal ganglia after intranasal infection (49). This makes it unlikely that the removal of the entire cluster of 11 PrV miRNA genes would make a difference for the ability of PrV to establish latency.

Transcriptional patterns of the PrV genome during latency. With the exception of the deleted miRNAs, the viral transcriptional profiles of ganglia latent for the mutant (M) PrV displayed only subtle differences compared to the parental WT virus. The finding that the levels of ex1/ex2 junction and exon 2 of LLT were

TABLE 4 Diseases and biofunctions in trigeminal ganglia latent for M or WT PrV

Disease(s) or biofunction(s)	*z* score for[a]: M vs C	*z* score for[a]: WT vs C	*P* value[b]	Genes
Inflammation of organ	−1.17	1.05	1.38E−03	AGT, CD8A, CXCL9, CXCL13, CYP2E1, GPD1, ICOS, SCARA5, TNFRSF10B, VIP
Inflammatory response	0.26	1.61	3.15E−03	AGT, CXCL13, CXCL9, ITGA2, PLA2G2D, SCARA5, VIP
Cell death of T lymphocytes	−0.42	0.91	9.16E−03	GZMA, ICOS, LAG3, VIP
Migration of dendritic cells	−0.69	0.44	**6.77E−06**	AGT, CXCL13, CXCL9, ICOS, VIP
Recruitment of cells	−0.10	0.93	1.79E−03	AGT, CD8A, CXCL9, CXCL13, VIP
Activation of T lymphocytes	0.52	1.56	2.45E−03	CD8A, GZMA, ICOS, LAG3, VIP
Recruitment of lymphocytes	0.25	1.10	**4.88E−05**	AGT, CD8A, CXCL9, VIP
Recruitment of granulocytes	−1.10	−0.25	1.57E−03	AGT, CD8A, CXCL9, VIP
Cell movement of leukocytes	−0.46	0.29	1.07E−03	AGT, CD8A, CXCL9, CXCL13, ICOS, LAG3, LTC4S, VIP
Survival of organism	−2.06	−1.34	**5.00E−04**	AGT, CD8A, CXCL9, GZMA, LAG3, RSAD2, SLC14A1, VIP
Infiltration by mononuclear leukocytes	−0.62	0.06	**6.45E−05**	AGT, CXCL9, ICOS, LAG3, VIP
Leukocyte migration	0.17	0.80	**6.04E−04**	AGT, CD8A, CXCL9, CXCL13, ICOS, ITGA2, LAG3, LTC4S, VIP
Infiltration of leukocytes	−0.94	−0.32	**4.68E−04**	AGT, CXCL9, ICOS, LAG3, LTC4S, VIP
Cell movement of T lymphocytes	−0.54	0.05	**1.43E−05**	AGT, CXCL9, CXCL13, ICOS, LAG3, VIP
Lymphocyte migration	0.25	0.77	**2.06E−05**	AGT, CD8A, CXCL9, CXCL13, ICOS, LAG3, VIP
Activation of cells	0.65	1.15	**3.02E−04**	AGT, CD8A, CXCL9, GABRA1, GZMA, ICOS, LAG3, PLA2G2D, TNFRSF10B, VIP
Activation of leukocytes	0.42	0.91	**6.25E−05**	AGT, CD8A, CXCL9, GZMA, ICOS, LAG3, PLA2G2D, TNFRSF10B, VIP
Quantity of IgG	2.19	2.19	4.04E−03	CXCL9, ICOS, IgJ, IGLL1/IGLL5, RSAD2
Binding of blood cells	1.87	1.87	2.44E−03	CXCL9, CXCL13, ICOS, ITGA2
Binding of cells	1.60	1.60	**2.87E−04**	AGT, CXCL9, CXCL13, ICOS, ITGA2, SCARA5, VIP
Differentiation of blood cells	0.42	0.42	4.51E−03	AGT, CD8A, ICOS, IGLL1/IGLL5, RSAD2, TNFRSF10B, VIP
Accumulation of leukocytes	−0.46	−0.46	**4.47E−04**	AGT, CXCL9, ICOS, ITGA2, LTC4S
Quantity of helper T lymphocytes	−0.57	−0.57	1.35E−03	CD8A, ICOS, LAG3, PLA2G2D
Activation of phagocytes	−0.69	−0.69	8.01E−03	AGT, GZMA, PLA2G2D, TNFRSF10B
Quantity of antigen presenting cells	−1.07	−1.07	4.34E−03	AGT, CXCL13, LTC4S, PLA2G2D
Transport of molecule	−1.22	−1.39	2.94E−03	AGT, CD8A, CGA, CYP2E1, EPHX1, GABRA1, ICOS, MX2, RSAD2, SLC14A1, VIP
Secretion of molecule	−1.22	−1.41	**4.84E−04**	AGT, CD8A, CGA, CYP2E1, ICOS, RSAD2, VIP
Flux of Ca^{2+}	0.91	0.54	**6.80E−04**	AGT, CD8A, CXCL13, ICOS, VIP
Cellular homeostasis	−0.29	−0.66	**4.68E−06**	AGT, CD8A, CXCL13, CYP2E1, GABRA1, GZMA, ICOS, LAG3, MTNR1B, PYGM, RSAD2, SCARA5, SLC14A1, TNFRSF10B, VIP
Production of reactive oxygen species	−0.09	−0.60	2.35E−03	AGT, CXCL9, CYP2E1, GZMA, VIP
Ion homeostasis of cells	0.25	−0.25	**9.97E−06**	AGT, CD8A, CXCL13, GABRA1, ICOS, PYGM, SCARA5, SLC14A1, VIP
Quantity of cells	0.42	−0.18	**7.95E−04**	AGT, CD8A, CGA, CXCL13, GABRA1, ICOS, IgJ, IGLL1/IGLL5, LAG3, LTC4S, PLA2G2D, SLC14A1, VIP
Quantity of blood cells	0.78	0.14	**1.32E−04**	AGT, CD8A, CXCL13, ICOS, IgJ, IGLL1/IGLL5, LAG3, LTC4S, PLA2G2D, SLC14A1, VIP
Mobilization of Ca^{2+}	0.18	−0.46	**2.74E−04**	AGT, CD8A, CXCL9, CXCL13, NPSR1, VIP
Quantity of leukocytes	0.58	−0.07	**2.09E−04**	AGT, CD8A, CXCL13, ICOS, IgJ, IGLL1/IGLL5, LAG3, LTC4S, PLA2G2D, VIP
Quantity of lymphocytes	0.98	0.26	**1.31E−04**	AGT, CD8A, CXCL13, ICOS, IgJ, IGLL1/IGLL5, LAG3, PLA2G2D, VIP
Quantity of T lymphocytes	0.02	−0.85	3.46E−03	AGT, CD8A, ICOS, LAG3, PLA2G2D, VIP
Proliferation of lymphocytes	1.97	1.03	3.33E−03	BTNL9, CD8A, ICOS, IGLL1/IGLL5, LAG3, TNFRSF10B, VIP
Quantity of Ca^{2+}	0.99	0.01	4.55E−03	AGT, CD8A, CXCL9, CXCL13, VIP
Synthesis of fatty acid	−0.14	−1.14	7.55E−03	AGT, CYP2E1, LTC4S, PLA2G2D
Stimulation of cells	0.88	−0.13	**8.85E−04**	AGT, BTNL9, CD8A, ICOS, VIP
Expansion of T lymphocytes	1.70	0.27	**3.88E−04**	BTNL9, ICOS, LAG3, VIP
Concn of fatty acid	−0.28	−1.94	5.64E−03	AGT, CYP2E1, LTC4S, VIP

[a] The M versus C and WT versus C columns report the IPA *z* scores of activation (positive values) or inhibition (negative values) in the two comparisons. The most different ones are reported in boldface at the top (more inhibited/less activated in M) and bottom (more activated/less inhibited in M).
[b] The most significant *P* values of each biofunction are in boldface.

decreased in M ganglia (Fig. 7) is difficult to explain in the absence of any evidence of viral reactivation. In HSV, several results point to products of the LAT locus functioning in the repression of lytic gene expression, which would favor the establishment and maintenance of latency, and LAT has been proposed to silence viral gene expression as a long noncoding RNA (50–52). However, in HSV the number of neurons harboring virus is decreased after infection by ΔLAT mutants, as reviewed previously (53), while ganglia latent for the mutant PrV (M ganglia) carried amounts of latent PrV genomes similar to those of WT ganglia (Fig. 5). Decreased levels of LLT in ganglia latent for the nine-miRNA-deleted virus also are inconsistent with the predicted ability of multiple PrV miRNAs to target LLT as well as IE180 and EP0 (23). Finally, given the limited knowledge of the PrV LAT locus, we cannot

totally exclude that the 2.5-kb deletion removed regulatory sequences which may affect LLT expression in neurons (54).

In addition to LLT, all of the PrV miRNAs previously described from productively infected cells (22, 23) were detected in latent ganglia. The two most abundant miRNAs in WT ganglia, prv-miR-LLT1-3p and prv-miR-LLT2-5p, which are absent from the mutant PrV genome, are highly expressed during productive infection in PK15 cells (Table 2 and Fig. 6). Prv-miR-LLT1 is also the most highly expressed PrV miRNA in dendritic cells (22) and is the only one detected in trigeminal ganglia of pigs during acute infection, albeit at reduced sequencing depth (48). It is interesting that prv-miR-LLT10-3p, which maps outside the deleted region, was expressed by both M and WT virus at levels similar to those of prv-miR-LLT1-3p and prv-miR-LLT2-5p, which contrasts with the low expression of this miRNA during productive infection (Table 2 and Fig. 6). It should be noted that the gene coding for this miRNA is duplicated and maps at the 3′ end of both copies of IE180 (1). The fact that IE180 expression was not detected suggests that the mature prv-miR-LLT10 is expressed only by the miRNA gene copy adjacent to the LAT locus.

These findings suggest that, as for HSV (55), different PrV miRNAs are expressed preferentially during productive infection in cell culture and during latent infection in sensory ganglia. In this context, it is interesting that the only difference found was a transient upregulation of EP0 at 8 h p.i. (Fig. 3A and D) in PK15 cells infected by the mutant virus. Otherwise, the absence of miRNAs did not affect the replication properties of PrV (Fig. 2).

Transcriptional patterns of the host genome during latency. Our findings add to what had been proposed for HSV, i.e., that host parameters such as innate immunity (56), the repressive effects of immune cells in ganglia (57), and the neuronal environment (58) promote the establishment and maintenance of latency (52). Host genes which are differentially expressed during PrV latency are involved in biofunctions related to expansion, activation, and cell death of T lymphocytes and of dendritic cell migration. This parallels data from HSV latency, where the LAT locus has been shown to function as an immune evasion gene by promoting functional exhaustion of virus-specific $CD8^+$ T cells in latently infected trigeminal ganglia and by inhibiting the phenotypic and functional maturation of dendritic cells (59, 60).

Indeed, the most prominent differences between ganglia latent for the miRNA-deleted and parental PrV were found in host response, and, interestingly, without any evidence for differential expression of host miRNAs. Both viruses triggered a robust proinflammatory immune response (Fig. 9; also see Table S4 in the supplemental material), but a pronounced pattern of gene upregulation was found in ganglia latent for the mutant virus (Table 3; also see Table S3). The impairment of the host proinflammatory response is reflected by differential expression of a limited number of genes acting in several pathways (Table 4). VIP acts as an inhibitor in many biological functions. Its absence induces better Th1 polarization and antiviral immunity in mice (61), and VIP knockout mice have enhanced cellular immune responses and increased survival following murine cytomegalovirus infection (62). Various reports indicate CYP2E1 as a gene downregulated by various stimuli, including inflammation (63). Thus, in M ganglia VIP would be a factor of less efficient cell-mediated host response, and the upregulation of CYP2E1 would be a global indicator of reduced inflammatory response. Conversely, reduced levels of BTNL9 suggest a reduced ability of the mutant virus to control T cell activation (Table 4). The butyrophilin-like family encodes transmembrane glycoproteins with roles in immune coregulation and antigen presentation, and some of them are functionally implicated in T cell inhibition and in the modulation of epithelial cell-T cell interactions (64–66).

Overall, the pattern of gene upregulation found in the ganglia latent for the mutant virus is suggestive of a role for PrV miRNAs in regulating the host genome during latency. However, presumably only a fraction of the observed effects can be attributed to PrV miRNAs. Other regulatory sequences controlling the latent virus genome at the epigenetic level (54, 67) may map to the 2.5-kb region deleted from the PrV LAT locus and alter host transcription and immune responses. Additional functional studies are required to investigate the relative contribution of these different factors during PrV latency.

ACKNOWLEDGMENTS

We thank Laura Duciel for technical assistance, Nicolas Pollet for providing the PA-GFP-coilin C2 plasmid DNA, Florence Jaffrezic and Andrea Rau for help in statistical analysis, Jordi Estellé for help in setting up the RNA-seq analysis pipeline, Electra Tapanari for help with the 5′- and 3′-end gene data, and Maria Bernard for help in the database submission of sequencing data sets.

This work has benefited from the facilities and expertise of the IMAGIF platform (Centre de Recherche de Gif; https://www.imagif.cnrs.fr) and of the Genome and Transcriptome core facilities of the GenoToul platform (http://get.genotoul.fr).

The research leading to these results has received funding from the European Community's Seventh Framework Programme (FP7, 2007-2013), Research Infrastructures Action under grant agreement no. FP7-228394 (NADIR project), and by an INRA package grant (2011-2014) to E.G.

REFERENCES

1. **Klupp BG, Hengartner CJ, Mettenleiter TC, Enquist LW.** 2004. Complete, annotated sequence of the pseudorabies virus genome. J Virol **78:** 424–440. http://dx.doi.org/10.1128/JVI.78.1.424-440.2004.
2. **Szpara ML, Tafuri YR, Parsons L, Shamim SR, Verstrepen KJ, Legendre M, Enquist LW.** 2011. A wide extent of inter-strain diversity in virulent and vaccine strains of alphaherpesviruses. PLoS Pathog **7:**e1002282. http://dx.doi.org/10.1371/journal.ppat.1002282.
3. **Yu X, Zhou Z, Hu D, Zhang Q, Han T, Li X, Gu X, Yuan L, Zhang S, Wang B, Qu P, Liu J, Zhai X, Tian K.** 2014. Pathogenic pseudorabies virus, China, 2012. Emerg Infect Dis **20:**102–104. http://dx.doi.org/10.3201/eid2001.130531.
4. **Enquist LW.** 1994. Infection of the mammalian nervous system by pseudorabies virus (PRV). Semin Virol **5:**221–231. http://dx.doi.org/10.1006/smvy.1994.1024.
5. **Mettenleiter TC.** 2000. Aujeszky's disease (pseudorabies) virus: the virus and molecular pathogenesis–state of the art, June 1999. Vet Res **31:**99–115. http://dx.doi.org/10.1051/vetres:2000059.
6. **Pomeranz LE, Reynolds AE, Hengartner CJ.** 2005. Molecular biology of pseudorabies virus: impact on neurovirology and veterinary medicine. Microbiol Mol Biol Rev **69:**462–500. http://dx.doi.org/10.1128/MMBR.69.3.462-500.2005.
7. **Gutekunst DE, Pirtle EC, Miller LD, Stewart WC.** 1980. Isolation of pseudorabies virus from trigeminal ganglia of a latently infected sow. Am J Vet Res **41:**1315–1316.
8. **Cheung AK.** 1991. Cloning of the latency gene and the early protein 0 gene of pseudorabies virus. J Virol **65:**5260–5271.
9. **Priola SA, Gustafson DP, Wagner EK, Stevens JG.** 1990. A major portion of the latent pseudorabies virus genome is transcribed in trigeminal ganglia of pigs. J Virol **64:**4755–4760.
10. **Priola SA, Stevens JG.** 1991. The 5′ and 3′ limits of transcription in the pseudorabies virus latency associated transcription unit. Virology **182:** 852–856. http://dx.doi.org/10.1016/0042-6822(91)90628-O.
11. **Cheung AK.** 1989. Detection of pseudorabies virus transcripts in trigeminal ganglia of latently infected swine. J Virol **63:**2908–2913.

12. **Jin L, Scherba G.** 1999. Expression of the pseudorabies virus latency-associated transcript gene during productive infection of cultured cells. J Virol **73:**9781–9788.
13. **Bartel DP.** 2004. MicroRNAs: genomics, biogenesis, mechanism, and function. Cell **116:**281–297. http://dx.doi.org/10.1016/S0092-8674(04)00045-5.
14. **Yates LA, Norbury CJ, Gilbert RJ.** 2013. The long and short of microRNA. Cell **153:**516–519. http://dx.doi.org/10.1016/j.cell.2013.04.003.
15. **Mendell JT, Olson EN.** 2012. MicroRNAs in stress signaling and human disease. Cell **148:**1172–1187. http://dx.doi.org/10.1016/j.cell.2012.02.005.
16. **Skalsky RL, Cullen BR.** 2010. Viruses, microRNAs, and host interactions. Annu Rev Microbiol **64:**123–141. http://dx.doi.org/10.1146/annurev.micro.112408.134243.
17. **Cullen BR.** 2013. MicroRNAs as mediators of viral evasion of the immune system. Nat Immunol **14:**205–210. http://dx.doi.org/10.1038/ni.2537.
18. **Jurak I, Griffiths A, Coen DM.** 2011. Mammalian alphaherpesvirus miRNAs. Biochim Biophys Acta **1809:**641–653. http://dx.doi.org/10.1016/j.bbagrm.2011.06.010.
19. **Pfeffer S, Zavolan M, Grässer FA, Chien M, Russo JJ, Ju J, John B, Enright AJ, Marks D, Sander C, Tuschl T.** 2004. Identification of virus-encoded microRNAs. Science **304:**734–736. http://dx.doi.org/10.1126/science.1096781.
20. **Grundhoff A, Sullivan CS.** 2011. Virus-encoded microRNAs. Virology **411:**325–343. http://dx.doi.org/10.1016/j.virol.2011.01.002.
21. **Tang Q, Wu YQ, Chen DS, Zhou Q, Chen HC, Liu ZF.** 2014. Bovine herpesvirus 5 encodes a unique pattern of microRNAs compared with bovine herpesvirus 1. J Gen Virol **95:**671–678. http://dx.doi.org/10.1099/vir.0.061093-0.
22. **Anselmo A, Flori L, Jaffrezic F, Rutigliano T, Cecere M, Cortes-Perez N, Lefèvre F, Rogel-Gaillard C, Giuffra E.** 2011. Co-expression of host and viral microRNAs in porcine dendritic cells infected by the pseudorabies virus. PLoS One **6:**e17374. http://dx.doi.org/10.1371/journal.pone.0017374.
23. **Wu YQ, Chen DJ, He HB, Chen DS, Chen LL, Chen HC, Liu ZF.** 2012. Pseudorabies virus infected porcine epithelial cell line generates a diverse set of host microRNAs and a special cluster of viral microRNAs. PLoS One **7:**e30988. http://dx.doi.org/10.1371/journal.pone.0030988.
24. **Fuchs W, Backovic M, Klupp BG, Rey FA, Mettenleiter TC.** 2012. Structure-based mutational analysis of the highly conserved domain IV of glycoprotein H of pseudorabies virus. J Virol **86:**8002–8013. http://dx.doi.org/10.1128/JVI.00690-12.
25. **Kaplan AS, Vatter AE.** 1959. A comparison of herpes simplex and pseudorabies viruses. Virology **7:**394–407. http://dx.doi.org/10.1016/0042-6822(59)90068-6.
26. **Grimm KS, Klupp BG, Granzow H, Müller FM, Fuchs W, Mettenleiter TC.** 2012. Analysis of viral and cellular factors influencing herpesvirus-induced nuclear envelope breakdown. J Virol **86:**6512–6521. http://dx.doi.org/10.1128/JVI.00068-12.
27. **Mettenleiter TC.** 1989. Glycoprotein gIII deletion mutants of pseudorabies virus are impaired in virus entry. Virology **171:**623–625. http://dx.doi.org/10.1016/0042-6822(89)90635-1.
28. **Wernike K, Beer M, Freuling CM, Klupp B, Mettenleiter TC, Müller T, Hoffmann B.** 2014. Molecular double-check strategy for the identification and characterization of Suid herpes virus 1. J Virol Methods **209:**110–115. http://dx.doi.org/10.1016/j.jviromet.2014.08.022.
29. **Schroeder A, Mueller O, Stocker S, Salowsky R, Leiber M, Gassmann M, Lightfoot S, Menzel W, Granzow M, Ragg T.** 2006. The RIN: an RNA integrity number for assigning integrity values to RNA measurements. BMC Mol Biol **7:**3. http://dx.doi.org/10.1186/1471-2199-7-3.
30. **Thiery R, Pannetier C, Rziha HJ, Jestin A.** 1996. A fluorescence-based quantitative PCR method for investigation of pseudorabies virus latency. J Virol Methods **61:**79–87. http://dx.doi.org/10.1016/0166-0934(96)02072-1.
31. **Groenen MA, Archibald AL, Uenishi H, Tuggle CK, Takeuchi Y, Rothschild MF, Rogel-Gaillard C, Park C, Milan D, Megens HJ, Li S, Larkin DM, Kim H, Frantz LA, Caccamo M, Ahn H, Aken BL, Anselmo A, Anthon C, Auvil L, Badaoui B, Beattie CW, Bendixen C, Berman D, Blecha F, Blomberg J, Bolund L, Bosse M, Botti S, Bujie Z, Bystrom M, Capitanu B, Carvalho-Silva D, Chardon P, Chen C, Cheng R, Choi SH, Chow W, Clark RC, Clee C, Crooijmans RP, Dawson HD, Dehais P, De Sapio F, Dibbits B, Drou N, Du ZQ, Eversole K, Fadista J, Fairley S, Faraut T, Faulkner GJ, Fowler KE, Fredholm M, Fritz E, Gilbert JG, Giuffra E, Gorodkin J, Griffin DK, Harrow JL, Hayward A, Howe K, Hu ZL, Humphray SJ, Hunt T, Hornshøj H, Jeon JT, Jern P, Jones M, Jurka J, Kanamori H, Kapetanovic R, Kim J, Kim JH, Kim KW, Kim TH, Larson G, Lee K, Lee KT, Leggett R, Lewin HA, Li Y, Liu W, Loveland JE, Lu Y, Lunney JK, Ma J, Madsen O, Mann K, Matthews L, McLaren S, Morozumi T, Murtaugh MP, Narayan J, Nguyen DT, Ni P, Oh SJ, Onteru S, Panitz F, Park EW, Park HS, Pascal G, Paudel Y, Perez-Enciso M, Ramirez-Gonzalez R, Reecy JM, Rodriguez-Zas S, Rohrer GA, Rund L, Sang Y, Schachtschneider K, Schraiber JG, Schwartz J, Scobie L, Scott C, Searle S, Servin B, Southey BR, Sperber G, Stadler P, Sweedler JV, Tafer H, Thomsen B, Wali R, Wang J, White S, Xu X, Yerle M, Zhang G, Zhang J, Zhao S, Rogers J, Churcher C, Schook LB.** 2012. Analyses of pig genomes provide insight into porcine demography and evolution. Nature **491:**393–398. http://dx.doi.org/10.1038/nature11622.
32. **Anders S, Huber W.** 2010. Differential expression analysis for sequence count data. Genome Biol **11:**R106. http://dx.doi.org/10.1186/gb-2010-11-10-r106.
33. **Trapnell C, Roberts A, Goff L, Pertea G, Kim D, Kelley DR, Pimentel H, Salzberg SL, Rinn JL, Pachter L.** 2012. Differential gene and transcript expression analysis of RNA-seq experiments with TopHat and Cufflinks. Nat Protoc **7:**562–578. http://dx.doi.org/10.1038/nprot.2012.016.
34. **Robinson MD, McCarthy DJ, Smyth GK.** 2010. edgeR: a Bioconductor package for differential expression analysis of digital gene expression data. Bioinformatics **26:**139–140. http://dx.doi.org/10.1093/bioinformatics/btp616.
35. **Martin M.** 2011. Cutadapt removes adapter sequences from high-throughput sequencing reads. EMBnet J **7:**e47786. http://dx.doi.org/10.14806/ej.17.1.200.
36. **Friedländer MR, Mackowiak SD, Li N, Chen W, Rajewsky N.** 2012. miRDeep2 accurately identifies known and hundreds of novel microRNA genes in seven animal clades. Nucleic Acids Res **40:**37–52. http://dx.doi.org/10.1093/nar/gkr688.
37. **Kozomara A, Griffiths-Jones S.** 2011. miRBase: integrating microRNA annotation and deep-sequencing data. Nucleic Acids Res **39:**D152–D157. http://dx.doi.org/10.1093/nar/gkq1027.
38. **Tombácz D, Tóth JS, Petrovszki P, Boldogkoi Z.** 2009. Whole-genome analysis of pseudorabies virus gene expression by real-time quantitative RT-PCR assay. BMC Genomics **10:**491. http://dx.doi.org/10.1186/1471-2164-10-491.
39. **Untergasser A, Nijveen H, Rao X, Bisseling T, Geurts R, Leunissen JA.** 2007. Primer3Plus, an enhanced web interface to Primer3. Nucleic Acids Res **35:**W71–W74. http://dx.doi.org/10.1093/nar/gkm306.
40. **Owczarzy R, You Y, Groth CL, Tataurov AV.** 2011. Stability and mismatch discrimination of locked Nucleic acid-DNA duplexes. Biochemistry **50:**9352–9367. http://dx.doi.org/10.1021/bi200904e.
41. **Chen C, Ridzon DA, Broomer AJ, Zhou Z, Lee DH, Nguyen JT, Barbisin M, Xu NL, Mahuvakar VR, Andersen MR, Lao KQ, Livak KJ, Guegler KJ.** 2005. Real-time quantification of microRNAs by stem-loop RT-PCR. Nucleic Acids Res **33:**e179. http://dx.doi.org/10.1093/nar/gni178.
42. **Lewis BP, Burge CB, Bartel DP.** 2005. Conserved seed pairing, often flanked by adenosines, indicates that thousands of human genes are microRNA targets. Cell **120:**15–20. http://dx.doi.org/10.1016/j.cell.2004.12.035.
43. **Grimson A, Farh KK, Johnston WK, Garrett-Engele P, Lim LP, Bartel DP.** 2007. MicroRNA targeting specificity in mammals: determinants beyond seed pairing. Mol Cell **27:**91–105. http://dx.doi.org/10.1016/j.molcel.2007.06.017.
44. **Loveland JE, Gilbert JG, Griffiths E, Harrow JL.** 2012. Community gene annotation in practice. Database (Oxford) **2012:**bas009. http://dx.doi.org/10.1093/database/bas009.
45. **Cohrs RJ, Randall J, Smith J, Gilden DH, Dabrowski C, van Der Keyl H, Tal-Singer R.** 2000. Analysis of individual human trigeminal ganglia for latent herpes simplex virus type 1 and varicella-zoster virus nucleic acids using real-time PCR. J Virol **74:**11464–11471. http://dx.doi.org/10.1128/JVI.74.24.11464-11471.2000.
46. **Keane TM, Goodstadt L, Danecek P, White MA, Wong K, Yalcin B, Heger A, Agam A, Slater G, Goodson M, Furlotte NA, Eskin E, Nellåker C, Whitley H, Cleak J, Janowitz D, Hernandez-Pliego P, Edwards A, Belgard TG, Oliver PL, McIntyre RE, Bhomra A, Nicod J, Gan X, Yuan W, van der Weyden L, Steward CA, Bala S, Stalker J, Mott R, Durbin R, Jackson IJ, Czechanski A, Guerra-Assunção JA, Donahue LR, Reinholdt LG, Payseur BA, Ponting CP, Birney E, Flint J, Adams DJ.** 2011. Mouse genomic variation and its effect on phenotypes and gene regulation. Nature **477:**289–294. http://dx.doi.org/10.1038/nature10413.
47. **Fagerberg L, Hallström BM, Oksvold P, Kampf C, Djureinovic D, Odeberg J, Habuka M, Tahmasebpoor S, Danielsson A, Edlund K, Asplund A, Sjöstedt E, Lundberg E, Szigyarto CA, Skogs M, Takanen JO, Berling H, Tegel H, Mulder J, Nilsson P, Schwenk JM, Lindskog C, Danielsson F, Mardinoglu A, Sivertsson A, von Feilitzen K, Forsberg M, Zwahlen M, Olsson I, Navani S, Huss M, Nielsen J, Ponten F, Uhlén M.**

2014. Analysis of the human tissue-specific expression by genome-wide integration of transcriptomics and antibody-based proteomics. Mol Cell Proteomics **13:**397–406. http://dx.doi.org/10.1074/mcp.M113.035600.
48. **Timoneda O, Núñez-Hernández F, Balcells I, Muñoz M, Castelló A, Vera G, Pérez LJ, Egea R, Mir G, Córdoba S, Rosell R, Segalés J, Tomàs A, Sánchez A, Núñez JI.** 2014. The role of viral and host microRNAs in the Aujeszky's disease virus during the infection process. PLoS One **9:**e86965. http://dx.doi.org/10.1371/journal.pone.0086965.
49. **Cheung AK.** 1996. Latency characteristics of an EPO and LLT mutant of pseudorabies virus. J Vet Diagn Investig **8:**112–115. http://dx.doi.org/10.1177/104063879600800119.
50. **Cliffe AR, Garber DA, Knipe DM.** 2009. Transcription of the herpes simplex virus latency-associated transcript promotes the formation of facultative heterochromatin on lytic promoters. J Virol **83:**8182–8190. http://dx.doi.org/10.1128/JVI.00712-09.
51. **Wang QY, Zhou C, Johnson KE, Colgrove RC, Coen DM, Knipe DM.** 2005. Herpesviral latency-associated transcript gene promotes assembly of heterochromatin on viral lytic-gene promoters in latent infection. Proc Natl Acad Sci U S A **102:**16055–16059. http://dx.doi.org/10.1073/pnas.0505850102.
52. **Kramer MF, Jurak I, Pesola JM, Boissel S, Knipe DM, Coen DM.** 2011. Herpes simplex virus 1 microRNAs expressed abundantly during latent infection are not essential for latency in mouse trigeminal ganglia. Virology **417:**239–247. http://dx.doi.org/10.1016/j.virol.2011.06.027.
53. **Roizman B, Whitley RJ.** 2013. An inquiry into the molecular basis of HSV latency and reactivation. Annu Rev Microbiol **67:**355–374. http://dx.doi.org/10.1146/annurev-micro-092412-155654.
54. **Bloom DC, Giordani NV, Kwiatkowski DL.** 2010. Epigenetic regulation of latent HSV-1 gene expression. Biochim Biophys Acta **1799:**246–256. http://dx.doi.org/10.1016/j.bbagrm.2009.12.001.
55. **Jurak I, Hackenberg M, Kim JY, Pesola JM, Everett RD, Preston CM, Wilson AC, Coen DM.** 2014. Expression of herpes simplex virus 1 microRNAs in cell culture models of quiescent and latent infection. J Virol **88:**2337–2339. http://dx.doi.org/10.1128/JVI.03486-13.
56. **Leib DA, Harrison TE, Laslo KM, Machalek MA, Moorman NJ, Virgin HW.** 1999. Interferons regulate the phenotype of wild-type and mutant herpes simplex viruses in vivo. J Exp Med **189:**663–672. http://dx.doi.org/10.1084/jem.189.4.663.
57. **Knickelbein JE, Khanna KM, Yee MB, Baty CJ, Kinchington PR, Hendricks RL.** 2008. Noncytotoxic lytic granule-mediated CD8+ T cell inhibition of HSV-1 reactivation from neuronal latency. Science **322:**268–271. http://dx.doi.org/10.1126/science.1164164.
58. **Kristie TM, Vogel JL, Sears AE.** 1999. Nuclear localization of the C1 factor (host cell factor) in sensory neurons correlates with reactivation of herpes simplex virus from latency. Proc Natl Acad Sci U S A **96:**1229–1233. http://dx.doi.org/10.1073/pnas.96.4.1229.
59. **Chentoufi AA, Kritzer E, Tran MV, Dasgupta G, Lim CH, Yu DC, Afifi RE, Jiang X, Carpenter D, Osorio N, Hsiang C, Nesburn AB, Wechsler SL, Benmohamed L.** 2011. The herpes simplex virus 1 latency-associated transcript promotes functional exhaustion of virus-specific CD8+ T cells in latently infected trigeminal ganglia: a novel immune evasion mechanism. J Virol **85:**9127–9138. http://dx.doi.org/10.1128/JVI.00587-11.
60. **Chentoufi AA, Dervillez X, Dasgupta G, Nguyen C, Kabbara KW, Jiang X, Nesburn AB, Wechsler SL, Benmohamed L.** 2012. The herpes simplex virus type 1 latency-associated transcript inhibits phenotypic and functional maturation of dendritic cells. Viral Immunol **25:**204–215. http://dx.doi.org/10.1089/vim.2011.0091.
61. **Li JM, Southerland L, Hossain MS, Giver CR, Wang Y, Darlak K, Harris W, Waschek J, Waller EK.** 2011. Absence of vasoactive intestinal peptide expression in hematopoietic cells enhances Th1 polarization and antiviral immunity in mice. J Immunol **187:**1057–1065. http://dx.doi.org/10.4049/jimmunol.1100686.
62. **Li JM, Darlak KA, Southerland L, Hossain MS, Jaye DL, Josephson CD, Rosenthal H, Waller EK.** 2013. VIPhyb, an antagonist of vasoactive intestinal peptide receptor, enhances cellular antiviral immunity in murine cytomegalovirus infected mice. PLoS One **8:**e63381. http://dx.doi.org/10.1371/journal.pone.0063381.
63. **Renton KW, Nicholson TE.** 2000. Hepatic and central nervous system cytochrome P450 are down-regulated during lipopolysaccharide-evoked localized inflammation in brain. J Pharmacol Exp Ther **294:**524–530.
64. **Henry J, Miller MM, Pontarotti P.** 1999. Structure and evolution of the extended B7 family. Immunol Today **20:**285–288. http://dx.doi.org/10.1016/S0167-5699(98)01418-2.
65. **Afrache H, Gouret P, Ainouche S, Pontarotti P, Olive D.** 2012. The butyrophilin (BTN) gene family: from milk fat to the regulation of the immune response. Immunogenetics **64:**781–794. http://dx.doi.org/10.1007/s00251-012-0619-z.
66. **Abeler-Dörner L, Swamy M, Williams G, Hayday AC, Bas A.** 2012. Butyrophilins: an emerging family of immune regulators. Trends Immunol **33:**34–41. http://dx.doi.org/10.1016/j.it.2011.09.007.
67. **Cliffe AR, Coen DM, Knipe DM.** 2013. Kinetics of facultative heterochromatin and polycomb group protein association with the herpes simplex viral genome during establishment of latent infection. mBio **4:**e00590-12. http://dx.doi.org/10.1128/mBio.00590-12.